Biosensors and Bioelectronics 213 (2022) 114453

Contents lists available at ScienceDirect

Biosensors and Bioelectronics

journal homepage: www.elsevier.com/locate/bios

Enzyme-embedded electrospun fiber sensor of hydrophilic polymer for fluorometric ethanol gas imaging in vapor phase

Kenta Iitani [a,b], Misa Nakaya [a], Tsubomi Tomono [a], Koji Toma [b], Takahiro Arakawa [b], Yuji Tsuchido [a], Kohji Mitsubayashi [b,c,*], Naoya Takeda [a,**]

[a] Department of Life Science and Medical Bioscience, Graduate School of Advanced Science and Engineering, Waseda University (TWIns), 2-2 Wakamatsu-cho, Shinjuku-ku, Tokyo, 162-8480, Japan
[b] Department of Biomedical Devices and Instrumentation, Institute of Biomaterials and Bioengineering, Tokyo Medical and Dental University (TMDU), 2-3-10 Kanda-Surugadai, Chiyoda-ku, Tokyo, 101-0062, Japan
[c] Graduate School of Medical and Dental Sciences, Tokyo Medical and Dental University (TMDU), 1-5-45 Yushima, Bunkyo-ku, Tokyo, 113-8510, Japan

ARTICLE INFO

Keywords:
Enzymatic biosensor
Electrospun fiber
Gas sensor
Fluorescence imaging
Hydrophilic polymer

ABSTRACT

Non-invasive measurement of volatile organic compounds (VOCs) emitted from living organisms is a powerful technique for diagnosing health conditions or diseases in humans. Bio-based gas sensors are suitable for the sensitive and selective measurement of a target VOC from a complex mixture of VOCs. Conventional bio-based sensors are normally prepared as wet-type probes to maintain proteins such as enzymes in a stable state, resulting in limitations in the commercialization of sensors, their operating environment, and performance. In this study, we present an enzyme-based fluorometric electrospun fiber sensor (eFES) mesh as a gas-phase biosensor in dry form. The eFES mesh targeting ethanol was fabricated by simple one-step electrospinning of polyvinyl alcohol with an alcohol dehydrogenase and an oxidized form of nicotinamide adenine dinucleotide. The enzyme embedded in the eFES mesh worked actively in a dry state without pretreatment. Substrate specificity was also maintained, and the sensor responded well to ethanol with a sufficient dynamic range. Adjustment of the pH and coenzyme quantity in the eFES mesh also affected enzyme activity. The dry-form biosensor—eFES mesh—will open a new direction for gas-phase biosensors because of its remarkable performance and simple fabrication, which is advantageous for commercialization.

1. Introduction

There is a high demand for facile, selective, and sensitive measurements of volatile organic compounds (VOCs) in the gas phase. Numerous applications are conceivable: monitoring the natural environment (Sparks et al., 2012), industrial facilities (Cotte-Rodríguez et al., 2006), biological conditions of crops (Fabbri et al., 2020), and livestock animals (Neethirajan, 2017). VOCs are also emitted from humans as exhaled breath (Vasilescu et al., 2021) and transdermal gas (Iitani et al., 2021) without being invasive. Recent advances in basic research have revealed relationships between specific human-derived VOCs (H-VOCs) and diseases (Broza et al., 2015; Djago et al., 2021; Giannoukos et al., 2019). If small, easy-to-use, high-performance VOC sensors are available, it would be possible to check for signs of metabolic abnormalities and diseases simply at home.

Exhaled breath and transdermal gas consist of more than 1000 ultra-low concentrations of VOCs (de Lacy Costello et al., 2014). Hence, H-VOCs are usually measured by gas analysis systems, such as gas chromatography-mass spectrometry, which possesses high selectivity and sensitivity (Beccaria et al., 2018). Gas-phase bio-based sensors using the molecular recognition ability of enzymes, antibodies, and peptides are considered suitable for the continuous and/or rapid measurement of exhaled breath and transdermal gas. Previously, we developed highly sensitive fluorometric gas-phase bio-based sensors (bio-sniffer (Arakawa et al., 2019) and sniff-cam (Iitani et al., 2020b)) based on the catalytic reaction of immobilized enzymes in an insoluble carrier. These sensors

* Corresponding author. Department of Biomedical Devices and Instrumentation, Institute of Biomaterials and Bioengineering, Tokyo Medical and Dental University, 2-3-10 Kanda-Surugadai, Chiyoda-ku, Tokyo, 101-0062, Japan.
** Corresponding author. Department of Life Science and Medical Bioscience, Graduate School of Advanced Science and Engineering, Waseda University (TWIns), 2-2 Wakamatsu-cho, Shinjuku-ku, Tokyo, 162-8480, Japan.
E-mail addresses: m.bdi@tmd.ac.jp (K. Mitsubayashi), ntakeda@waseda.jp (N. Takeda).

https://doi.org/10.1016/j.bios.2022.114453
Received 29 March 2022; Received in revised form 16 May 2022; Accepted 1 June 2022
Available online 7 June 2022

allow quantification of VOC concentrations by measuring the reduced form of nicotinamide adenine dinucleotide (NADH), which is a coenzyme of the enzymatic reaction. These measurements are based on its visible fluorescence (center wavelength of 460–490 nm) emitted during ultraviolet (UV) light (peak absorption wavelength of 340 nm) irradiation. While this series of gas-phase bio-based sensors successfully monitored metabolism based on H-VOC measurements, they have to overcome the common challenges of bio-based sensors, before they can become popular devices.

The first challenge is to design a substrate for enzyme immobilization. Bio-based sensors are usually fabricated by immobilizing proteins on a substrate (Zdarta et al., 2018) by additive methods such as physical adsorption, ionic bonding, and covalent bonding (Homaei et al., 2013). Some of the substrate materials and reagents used for immobilization show autofluorescence with UV light irradiation, which becomes background fluorescence. Removing undesired background fluorescence is one of the critical factors for achieving a highly sensitive fluorometric bio-based sensor. In addition, substrate structures can affect the diffusion of molecules to the biorecognition element (Gu et al., 2019); this in turn can affect the sensitivity and response time of gas-phase bio-based sensors. Bio-based sensors based on off-the-shelf substrates limit sensor performance because it is difficult to control their material characteristics and structure. Optimized substrates therefore need to be developed for specific applications. Gas-phase bio-based sensors ideally have a mesh-like structure with high air permeability.

The second challenge is the complexity of the bio-based sensor fabrication and operation process (Battat et al., 2022). Some procedures are difficult to automate for the immobilization of proteins that require careful handling, making it difficult to implement in the mass production process for commercialization. Typical proteins such as enzymes most actively function in the liquid phase. Therefore, even gas-phase bio-based sensors must operate under wet conditions. The bio-sniffer needs to use a pump to circulate NAD-containing buffer solution (Ye et al., 2015), which limits miniaturization. The enzyme-immobilized mesh of the sniff-cam was wetted by NAD solution immediately before the experiment (Iitani et al., 2019b). In addition, when measuring gaseous chemicals using a wetted sensor element, it is necessary to transfer molecules from the gas phase to the liquid phase (Lapshin et al., 2020; Yamada et al., 2021). The liquid layer may limit the sensor performance because of molecular transportation and solubility (Xing et al., 2021). Therefore, both the structure of the substrate and its condition (wet or dry) are important concerns in the development of gas-phase bio-based sensors.

To address these challenges simultaneously, we believe that bio-friendly electrospinning technology is promising (Nagase et al., 2017; Nagata et al., 2018; Takeda et al., 2016). Electrospinning is a method of converting polymer-containing solutions into fibers (Leach et al., 2010; Xue et al., 2019). The mainstream method for developing bio-based sensors using electrospinning is to immobilize proteins on the fiber surface (Liu et al., 2020; Tran and Balkus, 2012; Wang et al., 2009) rather than embedding them inside (Aldhahri et al., 2018; dos Santos et al., 2018; Tang et al., 2014). For instance, Li et al. reported a highly sensitive immunosensor fabricated with a titanium dioxide-based mesoporous electrospun nanofiber modified with octadecylphosphonic acid for the adsorption of antibodies on the fiber surface (Li et al., 2020). In addition, Jeong et al. developed a cortisol biosensor based on N-doped multidimensional carbon nanofibers fabricated *via* electrospinning, which allowed the detection at 10 aM of cortisol by immobilizing antibodies on its surface (Jeong et al., 2019). In these studies, fibrous materials with unique structures and functions were first fabricated by electrospinning, and then, proteins were immobilized on the surface to achieve outstanding functionality.

In contrast, our strategy is to fabricate a ready-to-use sensor in a single step to simplify the manufacturing and premeasurement processes. This is achieved by electrospinning a mixture of enzymes, coenzymes, and polymer solutions. In this process, an enzyme-embedded mesh with excellent air permeability is fabricated, which is suitable for a gas-phase sensor. The solvent of the polymer (and additive material) solution evaporates during the electrospinning processes (Uematsu et al., 2018). Therefore, the produced mesh is dry, which enhances the permeability of gaseous molecules. It is possible to use enzymes in bio-based sensors, even in the dry state, if the structure of the enzyme can be fixed in functional form. Few studies have shown that enzymes work in the dry state (Barzana et al., 1987; Dunn and Daniel, 2004). In addition, it has been reported that the functional groups in the environment around the enzyme affect stabilization of the structure (Badieyan et al., 2017). Thus, it is possible that enzymes embedded in dry fibers composed of polymers can also express their functions.

In this study, we first evaluated the autofluorescence and microscopic structure of electrospun meshes fabricated using five polymers. The catalytic activity of alcohol dehydrogenase (ADH) after embedding in the electrospun fiber was evaluated in the liquid phase. Subsequently, we tested the gaseous ethanol (EtOH) detection ability of ready-to-use enzyme-based fluorometric electrospun fiber sensor (eFES) meshes originating from ADH and cofactors. Finally, we investigated the possibility of quantitative imaging of gaseous EtOH after optimizing the reaction conditions of ADH, including the pH and quantity of coenzyme.

2. Experimental

2.1. Materials and reagents

The following polymers were selected as candidate materials to fabricate the eFES mesh. They were chosen following the maturation in fiber preparation by electrospinning in our previous studies, and preliminary experiments: poly-L-lactic acid (PLLA, molecular weight (MW): 90,000, cat#: 18582-1, Polysciences Inc., USA); polyglycolic acid (PGA, MW: > 100,000, cat#: 06525, Polysciences Inc., USA); poly (lactic-*co*-glycolic acid) (PLGA, lactide:glycolide = 75:25, M_w (weight averaged MW): 76,000–115,000, cat#: 719927, Sigma-Aldrich, USA); polycaprolactone (PCL, M_n (number averaged MW) 70,000–90,000, cat#: 440744, Sigma-Aldrich, USA); and polyvinyl alcohol (PVA, PVA mixture, mainly composed of PVA and water, cat#: NA-150, Yamato, Japan). Dichloromethane (DCM, purity ≥99.5%, cat#: 22415-13, Nakalai Tesque, Inc., Japan), hexafluoroisopropanol (HFIP, purity: 99%, cat#: PC4750, Apollo Scientific Ltd., UK), and acetone (purity ≥99.5%, cat#: 014-00347, Fujifilm Wako Pure Chemical Corp., Japan) were used to prepare the polymer solutions. ADH (321 units/mg, from *Saccharomyces cerevisiae*, cat#: A7011) was purchased from Sigma-Aldrich, USA. NAD^+ (cat#: 4405600) was purchased from Oriental Yeast (Japan). EtOH, methanol, 2-propanol, acetic acid, and sodium hydroxide were obtained from Fujifilm Wako Pure Chemical Corp., Japan.

2.2. Selection of optimum polymer material for eFES mesh

The fluorescence-based sensing principle of EtOH *via* the ADH-mediated redox reaction was used as a proof-of-concept model in this study (Fig. 1A). There are a wide variety of NADH-depended dehydrogenases (Sellés Vidal et al., 2018), which allows for the future versatility of gas-phase bio-based sensors based on this principle. Briefly, the oxidized form of NAD (NAD^+) is reduced to NADH when EtOH is catalyzed by ADH in an alkaline environment. In this reaction, only NADH showed fluorescence ($\lambda_{excitation}$ = 340 nm, $\lambda_{emission}$ = 490 nm). Since the concentration of the NADH produced is correlated to the concentration of the EtOH, sensors incorporating this principle can quantify the EtOH concentration by measuring the fluorescence originating from the NADH.

In the fabrication of electrospun meshes, PLLA, PGA, PLGA, and PCL were prepared with 10, 15, 20, and 8 w/v% of polymer solutions, respectively. They were dissolved in a DCM-HFIP mixture (8:2), HFIP, acetone, and HFIP, respectively. The polymer solutions were obtained

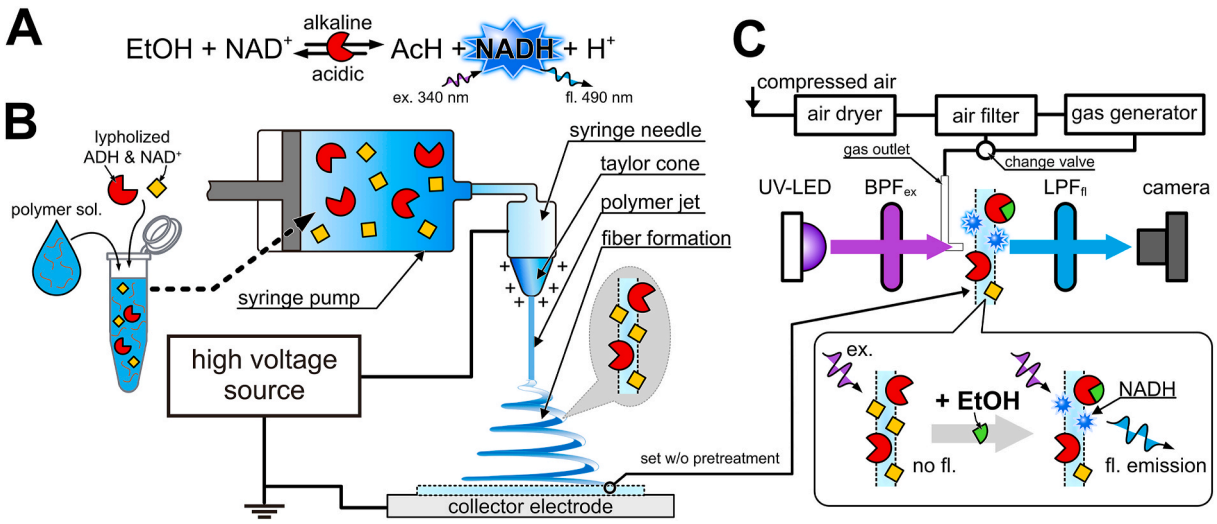

Fig. 1. (A) Detection principle of EtOH based on the ADH-mediated catalytic reaction. (B) Schematic diagram of the production of eFES mesh by electrospinning. (C) Experimental setup for measuring gaseous EtOH by fluorescence imaging using eFES mesh.

by stirring overnight at 23 °C. The PVA mixture was used as the original product. Five polymer solutions (0.6 mL) were injected into a disposable syringe (cat#: SS01-T, Terumo, Japan) and then set in an electrospinning system (NANON-03, MECC Corp., Japan) with a drum collector. The initial electrospinning conditions and parameters are presented in Table S1. These parameters were manually varied to obtain a stable polymer jet during electrospinning. Fig. 1B shows a schematic of the electrospinning process. Note that the ADH and NAD^+ were not present in the polymer solution used in this experiment.

Next, the autofluorescence of the electrospun meshes at wavelengths longer than 400 nm, emitted by irradiating the excitation light at a wavelength of 340 nm, was compared using an optical system (Fig. 1C). A UV-LED (λ_{peak}: 340 ± 5.5 nm, cat#: M340L4, Thorlabs, USA) was used as the excitation light source. A bandpass filter (BPF_{ex}, λ = 340 ± 42.5 nm, cat#: 46-439, Edmund Optics, USA) purifying the excitation light was put in front of the UV-LED. The distribution of autofluorescence emitted from the electrospun mesh was captured using a CMOS camera (1920 × 1200 pixels, cat#: CS235MU, Thorlabs, USA) and recorded on a computer. A C-mount lens (focal length: 16 mm, aperture: F1.4, cat#: M1614-MP2, CBC, Japan) with 4.5 mm of extension tube was used to optimize the field of view, working distance, and distortion of images. To capture only fluorescent light, a long-pass filter (LPF_{fl}, cut at a wavelength of 400 nm, cat#: 62-981, Edmund Optics, USA) was placed in front of the camera lens. An optical system was placed in a dark box. The mean value of the fluorescence intensity in a 15 mm × 15 mm region of interest (ROI) in the captured images was measured using ImageJ2 (Rueden et al., 2017) in the FIJI project.

The microscopic structure of the same meshes was then observed by scanning electron microscopy (SEM, VE-9800, Keyence, Japan) after Au sputtering using a magnetron sputtering system (MSP-10, Vacuum Device, Japan).

2.3. Evaluation of ADH activity in the liquid phase

ADH containing PCL and PVA solutions were prepared as follows. First, an 8% w/v PCL solution was prepared with HFIP. The PVA mixture was used as the original product. Next, 1 mg of lyophilized ADH powder was dissolved in 1 mL of Tris-HCl buffer solution (Tris, pH = 8.0, 0.1 M). Then, the ADH and polymer solutions were mixed at a ratio of 1:9 (v/v). In addition, PCL and PVA solutions without enzymes were prepared for the control experiments. The electrospinning was performed using a drum collector. The four fabricated mesh sheets were cut into 78.5 cm^2 which contained 7.2 units of ADH in a piece of mesh. Each mesh was soaked in a reaction reagent (1 M EtOH and 1 mM NAD^+ in 1 mL of Tris at pH = 9.0, 0.1 M) and then shaken for 10 min at 23 °C. Subsequently, the mesh was removed from the reaction mixture. The absorption spectrum of the reacted solution was measured using a UV–Vis spectrophotometer (V-660, JASCO, Japan) at a constant temperature (20 °C). In addition, a fluorescence image of the reacted solutions in the cuvettes was captured under UV (365 nm) irradiation.

2.4. Bio-fluorometric gaseous EtOH imaging

A ready-to-use eFES mesh was fabricated by electrospinning an ADH and NAD^+ mixture containing PVA. To prepare the electrospinning solution for one eFES mesh, the lyophilized powder of 100 units ADH and 5 μmol NAD^+ were added to 50 μL of PVA and then mixed gently. For the control experiment, an eFES mesh without ADH was also prepared. The electrospun fiber was collected by a 3D printed holder covered with aluminum foil to add conductivity, with a 15 mm × 15 mm square hole (see Fig. S1). The fabricated mesh was installed in the experimental system (Fig. 1C) without any further treatment. Standard EtOH gas was applied from a gas outlet composed of a Pasteur glass tube placed 2 mm behind the eFES mesh. Standard EtOH gas was prepared using a standard gas generator (PD-1B, Gastec Corp., Japan) with dry and clean carrier air. The gas application procedure was as follows. (I) No air was applied 0–20 s after starting the video recording (30 fps). (II) Then, 200 ppm EtOH gas was applied to the eFES mesh for 20 s at a flow rate of 100 mL/min. (III) Dry and clean air was then applied at a flow rate of 100 mL/min. The control experiment was also conducted by applying dry and clean air at a flow rate of 100 mL/min instead of 200 ppm EtOH at step (II).

The mean fluorescence intensity (I_n) was calculated from 250 × 250 pixels of an ROI in each recorded image (*n*th). The average value of the mean fluorescence intensity for 0–20 s, which is the time without gas application, was defined as the baseline (I_0). The change in the fluorescence intensity (ΔI_n) was calculated as the difference between I_0 and I_n. The rate of fluorescence change, which is the reaction rate of ADH, was also calculated by using the differentiation operation with dt = 5 s.

2.5. Optimization of pH, NAD^+ and ADH

First, the pH values of the PVA mixtures were adjusted to 5, 6, 7, 8, 9, 10, and 11 by adding a sodium hydroxide solution (1 M in pure water). eFES meshes at different pH values were prepared by electrospinning an eFES solution, which was a mixture of ADH, NAD^+, and pH-adjusted

PVA. The quantities of ADH and NAD^+ in the 15 mm × 15 mm of eFES mesh were 100 units and 1 μmol, respectively. The effect of pH on the ADH activity in the eFES mesh was evaluated by applying 200 ppm EtOH. Statistical analyses of the gas-sensing data were performed using one-way ANOVA and Turkey-Kramer test with R software at a significance of $p < 0.05$. The gas application procedure was the same as that described in the previous section. A small piece of each eFES mesh was examined using SEM.

Next, the effect of NAD^+ on the eFES mesh was evaluated. The quantities of NAD^+ in eFES were 0.1, 1, and 10 μmol. The pH of the PVA mixture was adjusted to 8.0. The electrospun eFES mesh contained 100 units of ADH. The gas application procedure was the same as described in the previous section.

The effect of the quantity of ADH in the eFES mesh was then evaluated. The quantity of ADH varied between 50, 100, and 200 units per single eFES mesh (15 mm × 15 mm). The pH of the PVA mixture was adjusted to 8.0. The quantity of NAD^+ used was 10 μmol per mesh. The gas application procedure was the same as described in the previous section.

2.6. eFES mesh quantitative evaluation and selectivity

In this experiment, the quantity of EtOH molecules applied to the eFES mesh was controlled to evaluate the sensing ability of the mesh. The eFES mesh was prepared by electrospinning ADH (50 units) and NAD^+ (10 μmol) mixed with 50 μL of PVA (pH = 8.0). The concentration of EtOH gas and application time were fixed at 200 ppm and 20 s, respectively. The flow rates were set to 20, 50, 100, and 200 mL/min. As a result of a simple calculation, the numbers of gaseous EtOH molecules applied to the eFES mesh for 20 s were 2.7, 6.8, 13.6, and 27.3 nmol/s, respectively.

Selectivity compared to EtOH was also tested using typical VOCs found in exhaled air and transdermal gas (acetic acid, 2-propanol, acetone, and methanol). The concentrations of acetic acid, 2-propanol, acetone, and methanol were set at 1.0, 1.0, 1.5, and 1.0 ppm, respectively. The gas application method was the same as that used in the biofluorometric EtOH imaging section above, replacing EtOH with the VOC molecules.

3. Results and discussion

3.1. Evaluation of electrospun mesh characteristics

All the polymer solutions used in this study enabled the production of an electrospun mesh. Fig. 2A shows the results of SEM observations of the fiber shape and mesh structure made from PCL, PLGA, and PVA mixtures. A uniform mesh with a fiber diameter of approximately 1 μm was produced using each of the above polymers. The images shown as insets in Fig. 2B are autofluorescence obtained by irradiating excitation light (λ = 340 nm) on commercial cotton mesh and electrospun mesh made of PVA mixture. The cotton mesh was used as a substrate for enzyme immobilization in previous studies (Arakawa et al., 2015, 2017; Iitani et al., 2017b, 2018, 2019a, 2019b, 2020a, 2020b). The average autofluorescence intensity was calculated from the images of meshes made with different polymers (Fig. S2) whose values were then compared (Fig. 2B). The electrospun meshes showed lower autofluorescence compared to cotton mesh, which is a great advantage for fluorometric bio-based sensors. The PLLA electrospun mesh exhibited the lowest autofluorescence, which was 72% lower than that of the cotton mesh. However, PLLA was not used in the further experiments because it could not be mixed with the enzyme solution due to solubility. PLGA showed autofluorescence intermediate between PGA and PLLA. This result suggests that it is possible to precisely control the mechanical and chemical properties that are important for bio-based sensor development by designing polymers from the electrospinning materials. Among these candidates, PCL and PVA were selected for subsequent studies. PLGA was not selected because of the difficulty in stable electrospinning and large variation in fiber diameter. PGA was not selected because of its high autofluorescence.

3.2. Activity of ADH

Fig. 3 shows the absorption spectra of the reacted solution with ADH-containing electrospun meshes prepared with PCL or the PVA mixture. An absorption band derived from NADH was observed around 340 nm only in the ADH-containing electrospun mesh made of the PVA mixture (PVA/ADH mesh). Changes in absorbance according to EtOH concentration were observed using PVA/ADH meshes. In addition, NADH absorption was not observed when the PVA mesh without ADH was immersed in the reaction solution. These results indicated that the enzymatic activity of ADH can be maintained even after electrospinning with a PVA mixture. In contrast, no absorption bands of NADH were observed in the PCL/ADH mesh. There are two possible causes of enzyme deactivation during the electrospinning process: denaturation due to exposure of ADH to organic solvents, and high voltage. ADH activity was maintained by electrospinning with PVA mixture using water as the solvent, which suggests that the enzyme deactivation in PCL/ADH was caused by an organic solvent rather than a high voltage. The inset image in Fig. 3 was obtained by irradiating the solution with UV light at a wavelength of 365 nm after measuring the absorption

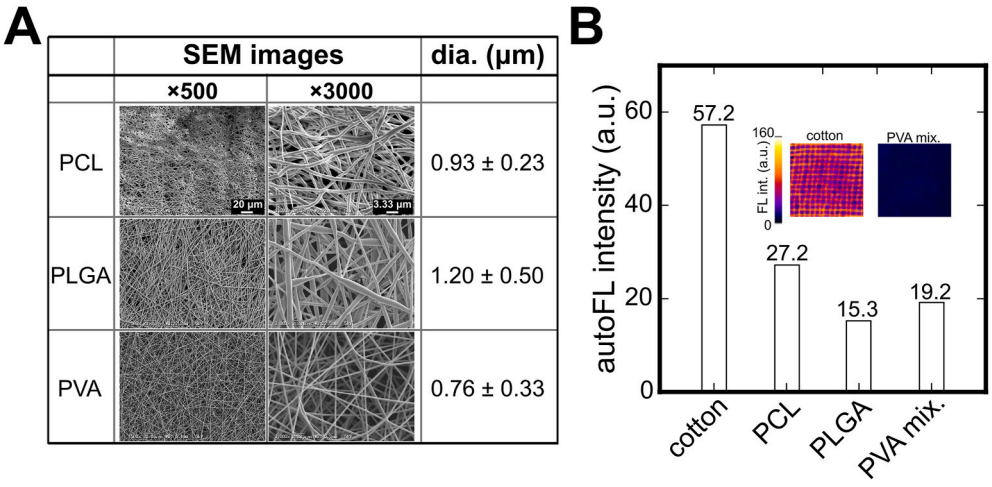

Fig. 2. (A) Typical SEM images of electrospun fiber meshes made from PCL, PLGA, and PVA. Magnifications of SEM images were as indicated. (B) Comparison of autofluorescence between cotton, PCL, PLGA, and PVA mixture. Inset images mapped autofluorescence intensity as pseudo color according to the color bar.

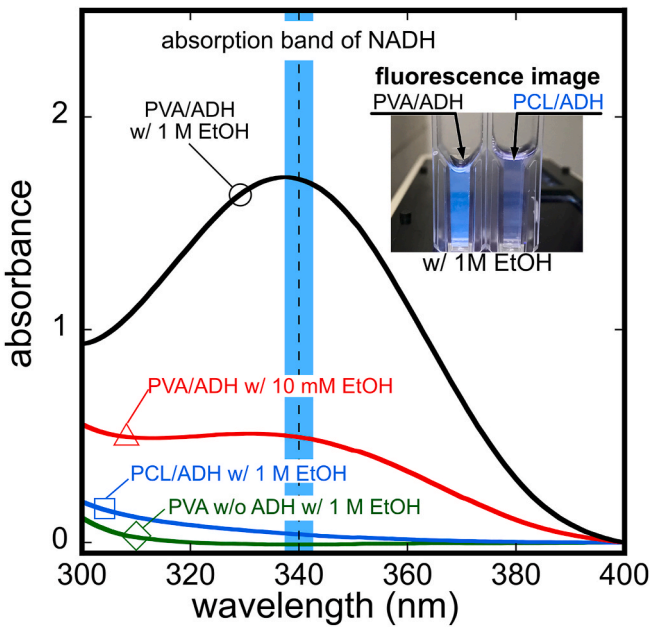

Fig. 3. Comparison of absorption spectra among a reacted solution of (○) PVA/ADH w/1 M of EtOH, (△) PVA/ADH w/10 mM of EtOH, (□) PCL/ADH w/1 M of EtOH, and (⋄) PVA w/o ADH w/1 M EtOH. The reaction time was fixed at 10 min among all samples. The inset image shows fluorescence of the reacted solution with 1 M EtOH of PVA/ADH and PCL/ADH under UV (λ = 365 nm) irradiation captured by a smartphone camera.

spectrum. Blue fluorescence, which matches the fluorescence wavelength of NADH (λ = 460–490 nm), was observed only for PVA/ADH. These data support the hypothesis that NADH was generated by the catalytic reaction of ADH in PVA/ADH. Based on the results, a ready-to-use eFES mesh made of a PVA mixture was investigated in the following experiments.

3.3. Imaging of EtOH by ADH and NAD^+

To accurately observe the change in the distribution of VOCs over time, it is important that the gas-sensing element itself has high permeability. In previous studies, enzyme-immobilized meshes were used for imaging VOCs when they were sufficiently wetted with an NAD^+ solution. In this case, the VOCs could be absorbed by the water contained in the mesh and diffused, making it difficult to accurately evaluate the distribution of the VOCs. In this experiment, we examined the usefulness of an eFES mesh as a gas-imaging element. Fig. 4A shows fluorescence images at −20, 0, 10, and 90 s extracted from the recorded video (see Supplemental Video 1) obtained by 200 ppm gaseous EtOH application to the PVA/ADH/NAD^+ eFES mesh from the backside. The colors in this fluorescence image correspond to the color bars indicating the fluorescence intensity. In gas imaging with the previous system, the fluorescence distribution was observed to spread in concentric circles around the gas application point. This was thought to be caused by the diffusion of VOCs by the liquid in the mesh. In contrast, in this experiment, the fluorescence distribution did not spread, and strong fluorescence was observed only at the gas application point within the eFES mesh. Fig. 4B shows the change in the average intensity over time, calculated from the fluorescence video. The sensor output ΔI was defined as the difference between the average value for 1.6–1.7 min and the baseline. The eFES mesh showed an increase in fluorescence intensity when EtOH gas was applied, whereas no increase in fluorescence intensity was observed when dry air was loaded onto the eFES mesh (negative control A). In addition, no increase in fluorescence was observed when gaseous EtOH was applied to the eFES mesh without ADH (negative control B). This suggested that the increase in fluorescence intensity when EtOH gas was applied to the eFES mesh was due to the enzymatic reaction of ADH.

The NADH produced remained in the mesh, and the fluorescence intensity did not drop down to its initial value even after EtOH gas was applied. To solve this issue, we applied the image differential analysis proposed in our previous study (Iitani et al., 2018) to the fluorescence video (Fig. 4C; see Supplemental Video 2).

Supplementary video related to this article can be found at https://doi.org/10.1016/j.bios.2022.114453.

In this method, the distribution of the ADH reaction rate, which

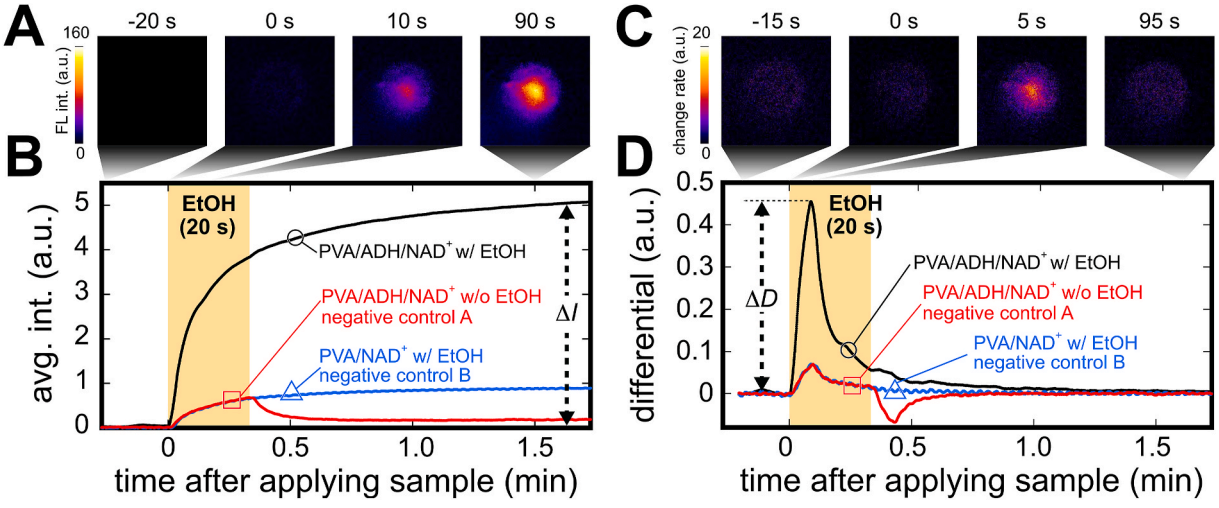

Fig. 4. Detection of 200 ppm gaseous EtOH applied for 20 s by eFES mesh (orange bands in B and D). (A) Fluorescence images representing the concentration distribution of gaseous EtOH at −20, 0, 10, and 90 s after starting EtOH application. (B) Time course of mean fluorescence intensity of ROI after starting EtOH application (or air). (○) PVA/ADH/NAD^+ w/EtOH; (△) PVA/NAD^+ w/EtOH; (□) PVA/ADH/NAD^+ w/o EtOH (air). The output signal ΔI was defined by averaging the fluorescence intensity from 1.6 to 1.7 min. (C) Resultant images of time domain-based differential analysis of fluorescence images at −15, 0, 5, and 95 s after starting EtOH application. (D) Time course of differential of fluorescence intensity or ROI after starting EtOH application (or air). (○) PVA/ADH/NAD^+ w/EtOH; (△) PVA/NAD^+ w/EtOH; (□) PVA/ADH/NAD^+ w/o EtOH (air). The output signal ΔD was defined as the difference between the peak max of the differential value and baseline (zero).

responds sensitively to EtOH concentration, was calculated. As a result of calculating the reaction rate, it was observed that the fluorescence change rate reached a peak (ΔD) with the application of gaseous EtOH to the eFES mesh, and then decreased (Fig. 4D). This decrease was probably caused by the lack of pre-doped NAD^+ owing to the reduction of almost all the NAD^+ around the gas application area during EtOH application.

Supplementary video related to this article can be found at https://doi.org/10.1016/j.bios.2022.114453.

3.4. Optimal pH, NAD^+ and ADH

We investigated the effect of the electrospinning solution pH on the enzymatic activity of the eFES mesh. The pH conditions did not notably affected shapes and diameters of the electrospun fibers (Fig. S3), ensuring almost equal gas permeabilities. Fig. 5A shows the relative values of ΔD obtained by EtOH application to the pH-adjusted eFES meshes (pH = 5, 6, 7, 8, 9,10, and 11), normalized by the strongest signal at pH 8. The statistical analysis using one-way ANOVA clearly showed significant difference in the whole data set. Subsequently conducted Turkey-Kramer test showed that differences on the signal values in the pairs of pH 6/pH 8 and pH 8/pH 11 were significant despite relatively large standard deviations, suggesting that the pH profile has a top around pH 8. This result is reasonable, considering that the optimal pH of ADH is 8.6–9.0 in the liquid phase (Iitani et al., 2017a). The actual pH of the electrospun fiber was unknown because of the lack of methods to measure it, but it was likely to be different from the pH of the prepared electrospinning solution owing to the volatilization of water in the PVA mixture during electrospinning. The change in enzyme activity with pH observed in this experiment was presumably due to the change in the higher-order structure of ADH (Raj et al., 2014). We assumed that the structure of ADH was fixed as a highly active and minimally hydrated state in the eFES mesh because the water volatilization during the electrospinning process would reduce the degree of freedom for structural change (Ohtake et al., 2011). It has been suggested that the air-liquid interface is a difficult environment for proteins such as enzymes (D'Imprima et al., 2019; Glaeser and Han, 2017). As PVA has a large number of OH groups, stabilization of the enzyme structure may have occured in the electrospun fiber, as shown in a previous study (Badieyan et al., 2017). Based on this result, the PVA mixture prepared at pH = 8.0 was used in the following experiments.

Fig. 5B shows the change in the fluorescence change rate over time when 200 ppm EtOH gas was applied to eFES meshes with NAD^+ quantities of 0.1, 1, and 10 μmol per mesh. An increase in ΔD was observed with an increase of the NAD^+ quantity in the eFES mesh (Fig. 5B inset). However, even at 10 μmol NAD^+, the fluorescence change rate started dropping down during EtOH gas loading (the area of orange band in Fig. 5B), as observed in Fig. 4D. A rate-limiting reaction due to the lack of NAD^+ seemed to occur. However, since more than 10 μmol of NAD^+ was not dissolved and a powdery mass was left, it was difficult to solve this issue by increasing the quantity of NAD^+ in the PVA mixture. Therefore, the quantity of NAD^+ per mesh was fixed at 10 μmol.

Fig. S4 shows the typical responses of the eFES mesh with different quantities of ADH (50, 100, and 200 units/mesh). The maximum value of ΔD did not change when the quantity of ADH per mesh was varied. Therefore, the quantity of ADH per mesh was fixed at 50 units in the subsequent experiment.

3.5. Quantitative and selective imaging of EtOH

Fig. 6A shows the relationship between ΔD and the molar quantity (2.7, 6.8, 13.6, and 27.3 nmol/s) of EtOH gas applied to the eFES mesh with the time course of fluorescence change rate (inset graph of Fig. 6A). When sufficient quantity of NAD^+ (10 μmol) was loaded in eFES mesh, it could quantitatively detect lower amount of EtOH gas (2.7–27.3 nmol/s for 20 s). The inset shows the fluorescence images obtained by applying gaseous EtOH at 6.8 and 27.3 nmol/s. Regardless of the quantity of EtOH applied, an increase in the fluorescence intensity was observed only at the gas loading point, suggesting that the quantitative imaging of gaseous EtOH under dry conditions could be possible. However, further studies are needed to determine the quantitative characteristics, such as robustness to ambient temperature and humidity disturbances (Yang and Russell, 1996a, 1996b). Furthermore, whether ΔD proportionally changes to the quantity of gaseous EtOH applied should be carefully examined to establish a practical calibration curve.

Fig. 6B shows the responses of the eFES mesh to EtOH, acetic acid, 2-propanol, acetone, and methanol. The signal was selectively obtained for EtOH. This suggests that not only the activity but also the substrate specificity of ADH was maintained in the eFES mesh after electrospinning. The high selectivity of the eFES mesh enables its use in gas mixtures, such as gaseous samples from living organisms, for future applications.

4. Conclusion

In this study, we developed a ready-to-use eFES mesh using an electrospinning technique applicable to the mass production. The bio-based sensor was designed to detect EtOH in the gas phase based on the fluorescence changes caused by ADH without pretreatment before measurement. First, we compared polymer materials for electrospinning

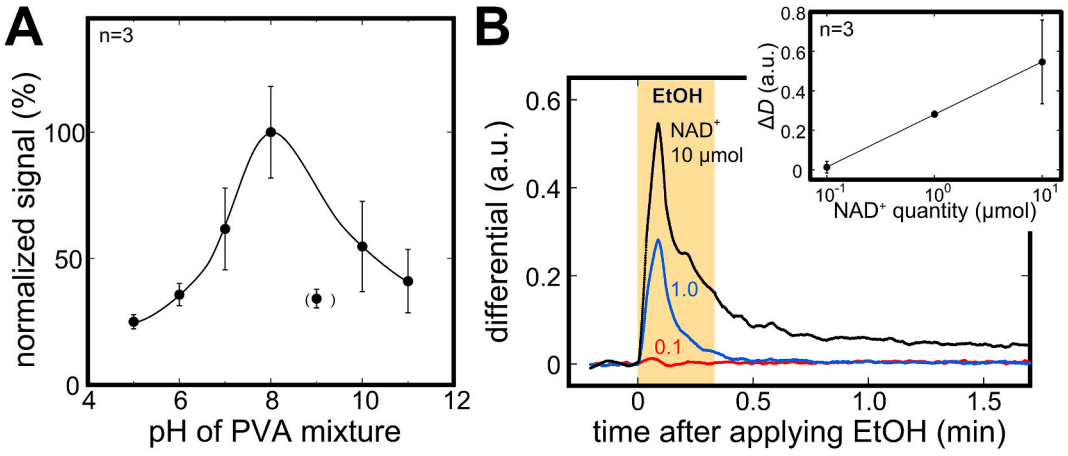

Fig. 5. (A) Dependence of ADH activity with EtOH on the pH of the PVA mixture used to immobilize ADH by electrospinning. The normalized signal of ΔD was plotted as a relative value of 100% at pH = 8.0. (B) Time course of differential signals that were obtained by applying gaseous EtOH (lasting for 20 s, orange band) to PVA/ADH/NAD^+ meshes with different quantities (0.1, 1.0, 10 μmol) of NAD^+. The inset graph showed a relationship between NAD^+ quantity in eFES mesh and ΔD.

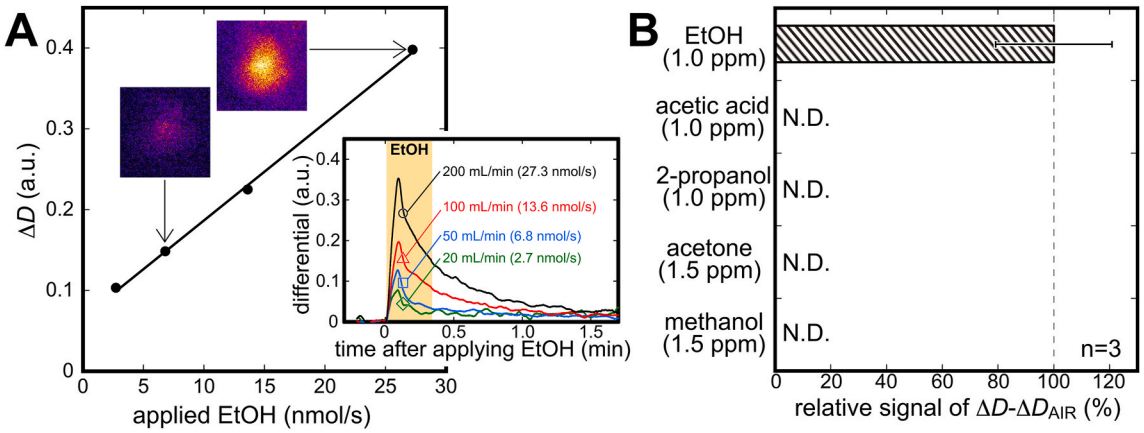

Fig. 6. (A) Relationship between the quantity of gaseous EtOH applied to eFES mesh and signal Δ*D*. Inset graph shows time course of differential signal with (◇) 2.7, (□) 6.8, (△) 13.6, and (○) 27.3 nmol/s of gaseous EtOH applied. (B) Selectivity of the eFES mesh tested with typical VOCs found in exhaled air and skin gas. N.D. was defined as a signal not detected.

in terms of autofluorescence, stability of electrospinning, and the possibility of retaining other materials, such as enzymes. By comparing different polymers, it was found that the PVA mixture, which was mainly composed of water and PVA, can be used to embed ADH in the fibers by electrospinning while maintaining a low background and enzyme activity. In addition, a ready-to-use eFES mesh, which can be used immediately after production without any pretreatment before use, was obtained by electrospinning the PVA mixture with ADH and NAD^+. The optimal conditions were experimentally determined for the pH of the PVA mixture and the quantities of ADH and NAD^+ added. The optimized eFES mesh generated fluorescence changes according to the number of EtOH molecules applied. In addition, no output was produced for VOCs, other than EtOH. These results suggest that hydrophilicity of the polymer substrate could be a crucial criterion to maintain enzymatic activity even in a vapor phase and the eFES mesh can be used as a sensor to measure the distribution of gaseous EtOH. To further improve the sensor performance, additional studies on optimization of the hydrophilic polymer materials, interaction between the polymer and enzyme, and the mechanism of maintaining enzyme activity in fibers are necessary. These studies are currently underway in our laboratories.

CRediT authorship contribution statement

Kenta Iitani: Conceptualization, Methodology, Software, Investigation, Writing – original draft, Funding acquisition. **Misa Nakaya:** Investigation, Writing – original draft. **Tsubomi Tomono:** Investigation, Writing – original draft. **Koji Toma:** Supervision. **Takahiro Arakawa:** Supervision. **Yuji Tsuchido:** Supervision, Writing – review & editing, Funding acquisition. **Kohji Mitsubayashi:** Conceptualization, Methodology, Supervision, Writing – review & editing. **Naoya Takeda:** Conceptualization, Methodology, Supervision, Writing – review & editing, Project administration, Funding acquisition.

Declaration of competing interest

The authors declare that they have no known competing financial interests or personal relationships that could have appeared to influence the work reported in this paper.

Acknowledgment

This work was supported by the Japan Society for the Promotion of Science (JSPS) Grants-in-Aid for Scientific Research (KAKENHI) grant numbers JP19J01649 and JP22K14267; The Ministry of Education, Culture, Sports, Science and Technology (MEXT) Special Funds for "Cooperative Research Project of Research Center for Biomedical Engineering"; the research grant from the Mitsubishi Materials-Faculty of Science and Engineering, Waseda University (2019); JST SCORE University Promotion Type, Grant Number JPMJST2053, Japan; the research grant from the Okawa Foundation for Information and Telecommunications (#21–10); and the Waseda University Grant for Special Research Projects (Project numbers: 2020Q-028 and 2021C-224). We would like to thank Editage (www.editage.com) for English language editing.

Appendix A. Supplementary data

Supplementary data to this article can be found online at https://doi.org/10.1016/j.bios.2022.114453.

References

Aldhahri, M.M., Almulaiky, Y.Q., El-Shishtawy, R.M., Al-Shawafi, W., Alngadh, A., Maghrabi, R., 2018. ACS Omega 3, 6346–6350.
Arakawa, T., Iitani, K., Wang, X., Kajiro, T., Toma, K., Yano, K., Mitsubayashi, K., 2015. Analyst 140, 2881–2886.
Arakawa, T., Sato, T., Iitani, K., Toma, K., Mitsubayashi, K., 2017. Anal. Chem. 89, 4495–4501.
Arakawa, T., Suzuki, T., Tsujii, M., Iitani, K., Chien, P.-J.J., Ye, M., Toma, K., Iwasaki, Y., Mitsubayashi, K., 2019. Biosens. Bioelectron. 129, 245–253.
Badieyan, S., Wang, Q., Zou, X., Li, Y., Herron, M., Abbott, N.L., Chen, Z., Marsh, E.N.G., 2017. J. Am. Chem. Soc. 139, 2872–2875.
Barzana, E., Klibanov, A.M., Karel, M., 1987. Appl. Biochem. Biotechnol. 15, 25–34.
Battat, S., Weitz, D.A., Whitesides, G.M., 2022. Lab Chip 22, 530–536.
Beccaria, M., Bobak, C., Maitshotlo, B., Mellors, T.R., Purcaro, G., Franchina, F.A., Rees, C.A., Nasir, M., Black, A., Hill, J.E., 2018. J. Breath Res. 13, 016005.
Broza, Y.Y., Mochalski, P., Ruzsanyi, V., Amann, A., Haick, H., 2015. Angew. Chem. Int. Ed. 54, 11036–11048.
Cotte-Rodríguez, I., Justes, D.R., Nanita, S.C., Noll, R.J., Mulligan, C.C., Sanders, N.L., Cooks, R.G., 2006. Analyst 131, 579.
D'Imprima, E., Floris, D., Joppe, M., Sánchez, R., Grininger, M., Kühlbrandt, W., 2019. Elife 8, 1–18.
de Lacy Costello, B., Amann, A., Al-Kateb, H., Flynn, C., Filipiak, W., Khalid, T., Osborne, D., Ratcliffe, N.M., 2014. J. Breath Res. 8, 014001.
Djago, F., Lange, J., Poinot, P., 2021. Nat. Rev. Chem 5, 183–196.
dos Santos, J.P., Zavareze, E. da R., Dias, A.R.G., Vanier, N.L., 2018. Int. J. Biol. Macromol. 118, 1676–1684.
Dunn, R.V., Daniel, R.M., 2004. Philos. Trans. R. Soc. Lond. Ser. B Biol. Sci. 359, 1309–1320.
Fabbri, B., Valt, M., Parretta, C., Gherardi, S., Gaiardo, A., Malagù, C., Mantovani, F., Strati, V., Guidi, V., 2020. Sensor. Actuator. B Chem. 303, 127227.
Giannoukos, S., Agapiou, A., Brkić, B., Taylor, S., 2019. J. Chromatogr. B 1105, 136–147.
Glaeser, R.M., Han, B.-G., 2017. Biophys. Reports 3, 1–7.
Gu, C., Hosono, N., Zheng, J.-J., Sato, Y., Kusaka, S., Sakaki, S., Kitagawa, S., 2019. Science 363, 387–391 (80).
Homaei, A.A., Sariri, R., Vianello, F., Stevanato, R., 2013. J. Chem. Biol. 6, 185–205.
Iitani, K., Chien, P.-J., Suzuki, T., Toma, K., Arakawa, T., Iwasaki, Y., Mitsubayashi, K., 2017a. ACS Sens. 2, 940–946.

Iitani, K., Hayakawa, Y., Toma, K., Arakawa, T., Mitsubayashi, K., 2019a. Talanta 197, 249–256.
Iitani, K., Naisierding, M., Toma, K., Arakawa, T., Mitsubayashi, K., 2020a. Analyst 145, 2915–2924.
Iitani, K., Ramamurthy, S.S., Ge, X., Rao, G., 2021. Curr. Opin. Biotechnol. 71, 198–205.
Iitani, K., Sato, T., Naisierding, M., Hayakawa, Y., Toma, K., Arakawa, T., Mitsubayashi, K., 2018. Anal. Chem. 90, 2678–2685.
Iitani, K., Sato, T., Naisierding, M., Hayakawa, Y., Toma, K., Arakawa, T., Mitsubayashi, K., 2017b. Analyst 142, 3830–3836.
Iitani, K., Toma, K., Arakawa, T., Mitsubayashi, K., 2020b. ACS Sens. 5, 338–345.
Iitani, K., Toma, K., Arakawa, T., Mitsubayashi, K., 2019b. Anal. Chem. 91, 9458–9465.
Jeong, G., Oh, J., Jang, J., 2019. Biosens. Bioelectron. 131, 30–36.
Lapshin, D.N., Jorge, M., Campbell, E.E.B., Sarkisov, L., 2020. J. Mater. Chem. 8, 11781–11799.
Leach, M.K., Feng, Z.Q., Tuck, S.J., Corey, J.M., 2010. J. Vis. Exp. 2–5.
Li, Z., Liu, Y., Chen, X., Cao, H., Shen, H., Mou, L., Deng, X., Jiang, X., Cong, Y., 2020. Biosens. Bioelectron. 166, 112444.
Liu, Yanbo, Hao, M., Chen, Z., Liu, L., Liu, Yao, Yang, W., Ramakrishna, S., 2020. Curr. Opin. Biomed. Eng. 13, 174–189.
Nagase, K., Sakurada, Y., Onizuka, S., Iwata, T., Yamato, M., Takeda, N., Okano, T., 2017. Acta Biomater. 53, 81–92.
Nagata, K., Kurebayashi, T., Imato, K., Takeda, N., 2018. J. Mater. Chem. B 6, 2052–2056.
Neethirajan, S., 2017. Sens. Bio-Sensing Res. 12, 15–29.
Ohtake, S., Kita, Y., Arakawa, T., 2011. Adv. Drug Deliv. Rev. 63, 1053–1073.
Raj, S.B., Ramaswamy, S., Plapp, B.V., 2014. Biochemistry 53, 5791–5803.
Rueden, C.T., Schindelin, J., Hiner, M.C., DeZonia, B.E., Walter, A.E., Arena, E.T., Eliceiri, K.W., 2017. BMC Bioinf. 18, 529.
Sellés Vidal, L., Kelly, C.L., Mordaka, P.M., Heap, J.T., 2018. Biochim. Biophys. Acta Protein Proteonomics 1866, 327–347.
Sparks, R.S.J., Biggs, J., Neuberg, J.W., 2012. Science 335, 1310–1311 (80).
Takeda, N., Tamura, K., Mineguchi, R., Ishikawa, Y., Haraguchi, Y., Shimizu, T., Hara, Y., 2016. J. Artif. Organs 19, 141–148.
Tang, C., Saquing, C.D., Sarin, P.K., Kelly, R.M., Khan, S.A., 2014. J. Membr. Sci. 472, 251–260.
Tran, D.N., Balkus, K.J., 2012. Top. Catal. 55, 1057–1069.
Uematsu, I., Uchida, K., Nakagawa, Y., Matsumoto, H., 2018. Ind. Eng. Chem. Res. 57, 12122–12126.
Vasilescu, A., Hrinczenko, B., Swain, G.M., Peteu, S.F., 2021. Biosens. Bioelectron. 182, 113193.
Wang, Z.-G., Wan, L.-S., Liu, Z.-M., Huang, X.-J., Xu, Z.-K., 2009. J. Mol. Catal. B Enzym. 56, 189–195.
Xing, Z., Hu, L., Ripatti, D.S., Hu, X., Feng, X., 2021. Nat. Commun. 12, 136.
Xue, J., Wu, T., Dai, Y., Xia, Y., 2019. Chem. Rev. 119, 5298–5415.
Yamada, T., Sugiura, H., Mimura, H., Kamiya, K., Osaki, T., Takeuchi, S., 2021. Sci. Adv. 7, 1–9.
Yang, F., Russell, A.J., 1996a. Biotechnol. Bioeng. 49, 700–708.
Yang, F., Russell, A.J., 1996b. Biotechnol. Bioeng. 49, 709–716.
Ye, M., Chien, P.-J., Toma, K., Arakawa, T., Mitsubayashi, K., 2015. Biosens. Bioelectron. 73, 208–213.
Zdarta, J., Meyer, A., Jesionowski, T., Pinelo, M., 2018. Catalysts 8, 92.